THE AMERICAN SOCIETY OF MECHANICAL ENGINEERS
345 E. 47 St., New York, N.Y. 10017

91-GT-84

The Effect of Tip Leakage Flow on Part-Load Performance of a Mixed-Flow Pump Impeller

AKIRA GOTO
Ebara Research Co., Ltd.
4-2-1 Honfujisawa
Fujisawa-shi 251
Japan

ABSTRACT

The flow phenomena around the positive slope region of the head-flow characteristic were investigated experimentally on a mixed-flow pump impeller at various tip clearances for both shrouded and unshrouded cases. A positively-sloped head-flow characteristic (abrupt decrease in pressure head) was caused by the onset of extensive flow separation in the impeller at the casing-suction surface corner. The corner separation in unshrouded cases appeared at much lower flow rate than the shrouded case due to the favorable effect of the tip leakage flow which displaced the wake region away from the corner. The interaction between the tip leakage flows and secondary flows and the formation of the wake regions in shrouded and unshrouded cases were explained based on experimental observation and computations by the Dawes' 3-D Navier-Stokes code. In the shrouded case, the flow rate, at which an abrupt decrease in pressure head appeared, was lowered substantially by introducing a leakage flow through a slit made between the shroud and the blade tip. Inlet recirculation was triggered by the corner separation and developed more gradually for larger tip clearances. Both the increased loss, due to the extensive flow separation, and the decreased Euler's head, due to the abrupt change in flow pattern caused by the inlet recirculation, were responsible for the generation of positively-sloped head-flow characteristic in the unshrouded case when the tip clearance was small, while the increased loss was the primary factor in the shrouded case.

NOMENCLATURE

C	absolute velocity
D_{eq}*	equivalent diffusion factor at blade tip
H	head
i	incidence angle (degree)
l_m	meridional chord length at midspan
n	number of blades
N	rotational speed (rev / min)
PS	pressure surface
Q	flow rate
Q*	flow rate ratio = Q /(Q at design point)
(r,θ,z)	cylindrical coordinates
R*	radius ratio = $(r - r_{hub})/(r_{shroud} - r_{hub})$
Re	Reynolds number = $W_1 l_m/\nu$
SS	suction surface
U	peripheral blade speed
U_{TE}	peripheral blade speed at midspan trailing edge
W	relative velocity
β	flow angle measured from circumferential direction
β_b	blade angle measured from circumferential direction
γ	stagger angle on mapped plane
ξ_τ	vorticity component perpendicular to stream line on stream surface
σ	solidity on mapped plane
ψ*	head coefficient = H / (U_{TE}^2/g)
ψ_e*	Euler's head coefficient
ψ_i*	total head coefficient at impeller exit
ψ_p*	pump head coefficient
ω	angular rotation frequency (radian / sec)

Subscripts

1	inlet
2	exit
m	meridional component
TE	impeller trailing edge
t	blade tip
u	circumferential component

Superscript

*	non-dimensional value (velocity and pressure head are normalized by U_{TE} and U_{TE}^2/g respectively)

INTRODUCTION

Mixed-flow pumps often show abrupt decrease in pressure head and positively-sloped head-flow characteristic when the flow rate is reduced below a critical value. In the present paper, this condition when the slope becomes positive will be referred to as "stall onset". Since the occurrence of positively-sloped characteristic is more likely to cause instabilities in a pumping system, it is usually a contractual requirement to guarantee a substantial margin between operating and stall points or to achieve a head-flow curve with a monotonously negative slope. Despite a lot of experimental investigations (e.g.

Presented at the International Gas Turbine and Aeroengine Congress and Exposition
Orlando, FL June 3-6, 1991
This paper has been accepted for publication in the Transactions of the ASME
Discussion of it will be accepted at ASME Headquarters until September 30, 1991

review by Engeda and Rautenberg, 1988), the flow phenomena under part-load operating condition and the generation mechanism of positively-sloped head-flow characteristic have not been well understood.

The performance difference between shrouded impellers (most commonly used for multistage configurations) and unshrouded impellers at various tip clearances is a great matter of interest, because they often show quite different characteristics, especially at partial flow rates. With regard to centrifugal impellers, Lenneman and Howard (1970), Howard and Kittmer (1975), Harada (1985), and Hamkins and Flack (1987) carried out comparison of internal flows between shrouded and unshrouded cases. Engeda and Rautenberg (1987) discussed the effect of tip clearance and reported that some impellers are highly sensitive to tip clearance. On the other hand, mixed-flow turbomachines are the least well understood machines, even around the design points, because of the complex three-dimensional flow fields caused by the strong interaction of secondary flows, and only a few studies have been done so far. Fraser et al. (1985) and Carey et al. (1986) measured the internal flows of mixed-flow fan impellers under various operating conditions using Laser-Doppler anemometry system. Based on these measurements, Carey et al. (1988) discussed the generation mechanism of positively-sloped head-flow characteristic curve. More recently, the author (Goto, 1990) investigated the formation of jet-wake flow patterns in a mixed-flow pump impeller at various tip clearances, including those in the shrouded case, by applying Dawes' 3-D Navier-Stokes code (Dawes, 1988) at 90% flow rate of the design point. The complex flow fields under part-load operation, including extensive flow separation and inlet/exit recirculation, seems to be practically still out of reach of numerical computations. However, a great deal of information, useful in understanding flow mechanics under part-load operation, were drawn from computations at higher flow rates. Goto (1990) also reported that the shrouded impeller showed positively-sloped head-flow characteristic at a much higher flow rate than that in unshrouded cases having the same blading.

In the present paper, the onset of positively-sloped head-flow characteristic in a mixed-flow pump impeller at various tip clearances, including that in the shrouded case, is investigated experimentally. The different mechanism of the onset of extensive flow separation and the production of positively-sloped characteristic is discussed based on Navier-Stokes computations by Goto (1990) at a higher flow rate and experimentally measured inlet/exit flow fields at lower flow rates. For the purpose of stability enhancement in shrouded impellers, the effect of a leakage flow through a slit along the shroud is also discussed in conjunction with the effect of inlet casing boundary layer.

EXPERIMENTAL APPARATUS AND METHOD

Mixed Flow Pump

Figure 1 schematically shows the test section of a mixed-flow pump used for performance tests and flow field measurements. The geometry of the impeller and design conditions are given in Table 1. The specific speed of the pump at its best efficiency point is $\omega\cdot\sqrt{Q}/(gH)^{3/4} = 1.34$, i.e. $N\cdot\sqrt{Q}/H^{3/4} = 548$ (rev/min, m^3/min, mH_2O). The pump was placed in a closed flow loop consisting of a 440mm-dia suction pipe, a 350mm-dia delivery pipe and a reservoir tank. Water was used as the test fluid and the flow rate was measured with venturi tubes and mercury manometers. The performance tests were conducted according to ISO standards. The impeller speed was 800 rev/min giving the Reynolds number of $Re = 1.33 \times 10^6$ at the design point.

The measurements were carried out on one impeller at five different tip clearances including the shrouded case, (S, U03, U05, U10 and U15): S represents the shrouded case, U03 the unshrouded case with a tip clearance of 0.3mm and so on. The unshrouded impeller was in fact a shrouded impeller with the front shroud removed. The tip clearance of the unshrouded impeller was adjusted by sliding the casing in the axial direction. Since the meridional shape of the blade tip was linear, the tip clearance was changed uniformly along the casing.

Table 1 Design of impeller

	hub	midspan	shroud	Number of blades : 5
β_{1b} (deg)	27.8	18.3	14.8	Design flow rate : 8.7 m^3 / min
β_{2b} (deg)	31.8	25.3	20.7	Design pump head : 7.0 mH_2O
r_1 (mm)	58.0	102.3	132.5	Rotational speed : 800 rev / min
r_2 (mm)	142.5	157.8	171.7	

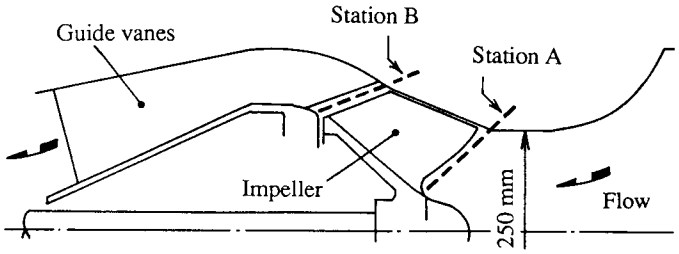

Fig.1 Mixed-flow pump geometry.

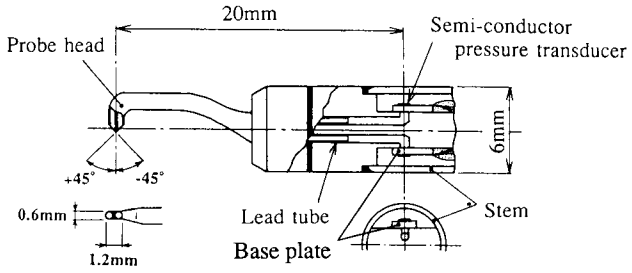

Fig.2 Construction of two-hole pitot probe.

Flow Field Measurements

Besides the performance tests, inlet and exit flow measurements of the impeller were carried out using two types of pressure probes. The inlet flow was measured by an ordinary three-hole cobra probe at Station A (Fig.1), 10mm upstream of the leading edge at midspan. On the other hand, the exit flow was measured by a two-hole pitot probe with high frequency response developed by Goto (1988) at Station B, 8mm downstream of the trailing edge. Figure 2 shows the construction of the two-hole pitot probe. Two diffusion type semi-conductor pressure transducers with a range of $-0.1 \sim 0.1$MPa and a frequency response of 100kHz were placed in the stem tube. Two pressure holes on the probe head were connected to the transducers by lead tubes of 0.4mm inside diameter filled with silicon oil. The resonance frequency of the pressure sensing system was about 5.6kHz and was high enough compared with the blade passing frequency of 67Hz.

The pitot probe was mounted on a traverse unit with two stepping motors controlled by a microcomputer and placed parallel to the blade trailing edge. The pressure fluctuation sensed by the pressure transducers was measured by a phase-locked multi-sampling and averaging technique. A set of 11 pressure data for each pressure hole, obtained at 11 probe setting angles over 450 sampling revolutions, were used to calculate the velocity vector and the static pressure from the calibration curves. Since the velocity vector and the static pressure were calculated using 4950 samples (=11 probe angle positions × 450 revolutions), the flow field was considered to be properly averaged in the statistical sense. Details on the measuring system and the data reduction method have been described in a previous paper by Goto (1988).

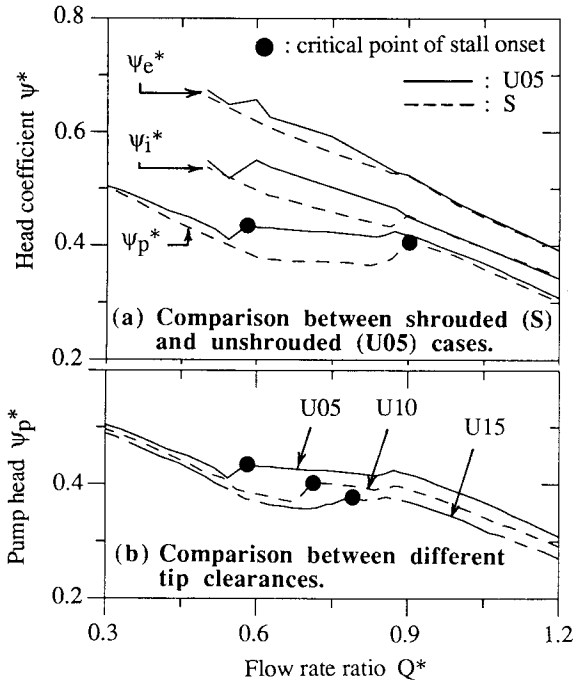

Fig.3 Head-flow characteristic curves.

Accuracy of Measurements

The probable uncertainty in the data reduction process and the measuring system of the two-hole pitot probe has been evaluated by Goto (1988) using a calibration test rig. The accuracy is ±2.5% in static pressure, ±1.3% in velocity, ±0.3 degrees in the yaw angle, and ±1 degree in the pitch angle. It has also been confirmed that the steady state calibration curves, obtained for uniform steady nozzle flows in the calibration rig, are correctly applicable to the present unsteady flow.

The drift of the pressure transducers between calibrations largely depends on the mounting condition of the gauges onto the base plates. The drift observed was less than 1% of the mean output voltage for 67 cases in 88 measured cases, while 5 cases revealed the drift of over 3%. The estimated maximum errors due to the drift are ±0.3% in static pressure, ±0.2% in velocity, ±0.01 degrees in the yaw angle, and ±1 degree in the pitch angle.

The flow rates measured by the pitot probe deviated −5.5% ±2.5% from those obtained by the venturi tubes. The error tends to increase as the flow rate is reduced. If we simply assume that the error in the initial setting of the probe yaw angle caused the bias of −5.5%, it corresponds to a 0.5 degree error.

FLOW PHENOMENA TOWARDS STALL

Head-Flow Characteristic Curve

Figure 3a compares the head-flow characteristic curves between the shrouded case S and the unshrouded case U05 (with a tip clearance of 0.5mm), and Fig.3b between cases with different tip clearances. Mass averaged Euler's head ψ_e* and the total head ψ_i*, obtained by exit flow measurements at Station B, are also presented in Fig.3a. All the cases exhibit positively-sloped head-flow characteristics (stall onset) when the flow rates are reduced below critical values (indicated by solid circles in Fig.3). At this critical point, similar flow pattern of an abrupt expansion of high loss region due to corner separation was observed at the exit of the impeller in every case. However, the dominant frequency of the flow field, after stall onset, was still the blade passing frequency and no evidence of rotating stall was found.

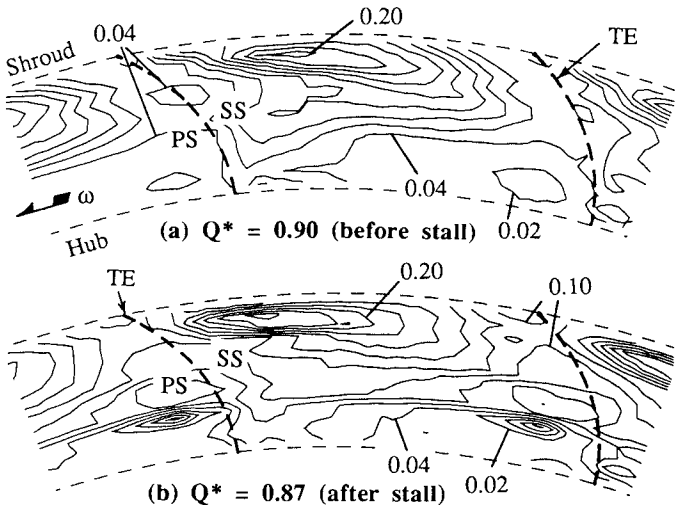

Fig.4 Exit loss distribution in shrouded case S. (Contour interval = 0.02)

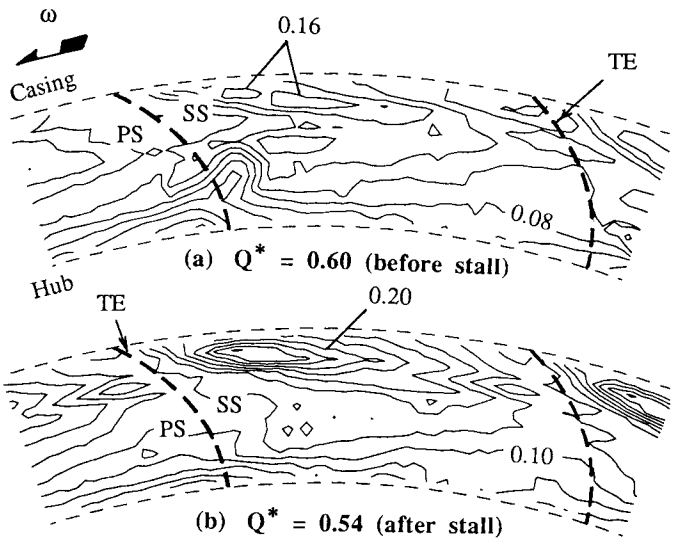

Fig.5 Exit loss distribution in unshrouded case U05. (Contour interval = 0.02)

Although the unshrouded impeller was in fact a shrouded impeller with the front shroud removed, the stall occurs at a much lower flow rate than in shrouded case S (Fig.3a). Head coefficients in case S are nearly equal to those in case U05 between Q*=0.9 and Q*=1.2. However, the total head ψ_i* at the exit of the impeller S drops suddenly at Q*=0.87, while the Euler's head ψ_e* is nearly the same with that in case U05. Figure 4 shows the contour maps of the loss on the quasi-orthogonal plane behind the impeller measured by the two-hole pitot probe. The loss is defined as the rothalpy difference between the measuring plane and the upstream of the impeller, where the flow is considered to be uniform. There is an abrupt expansion of the high loss region near the shroud-suction surface corner at Q*=0.87. From this, it is concluded that the positively-sloped characteristic in case S is mainly caused by a sudden increase in flow loss due to the onset of the extensive flow separation within the impeller. On the other hand, in the unshrouded case U05, the positively-sloped curve appears at a much lower flow rate of Q*=0.54

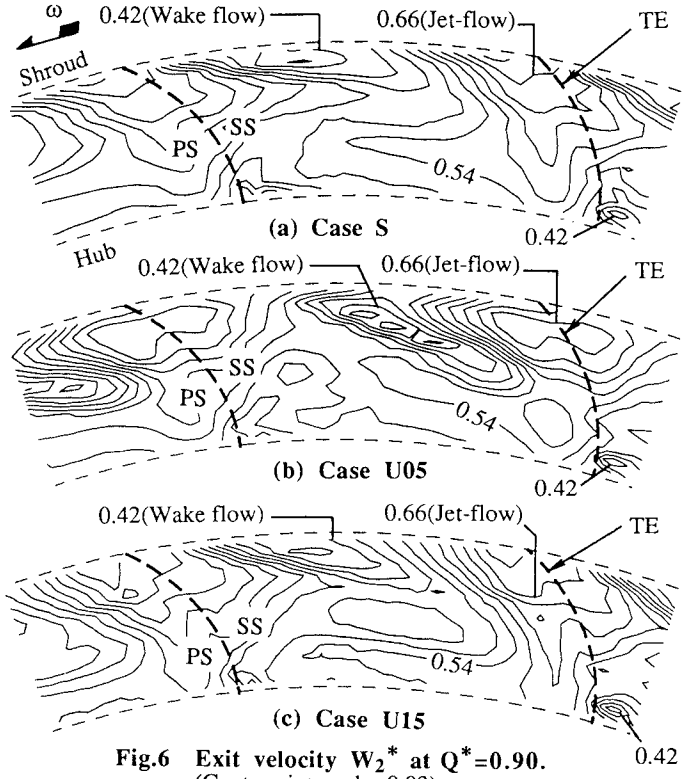

Fig.6 Exit velocity W_2^* at Q^*=0.90.
(Contour interval = 0.03)

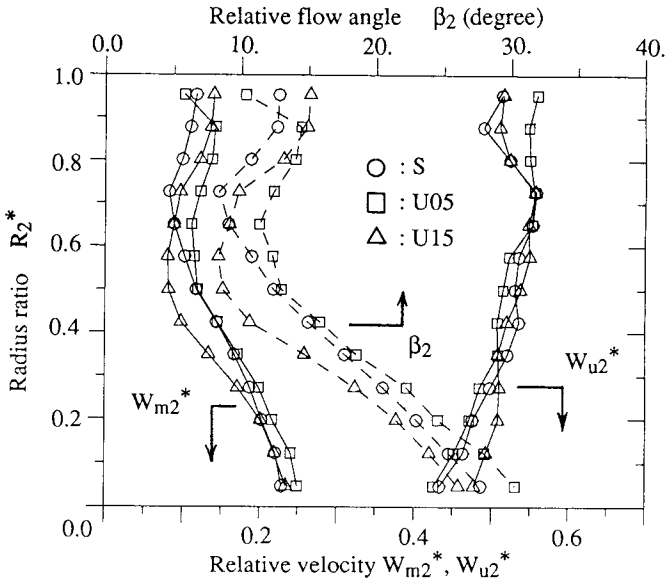

Fig.7 Exit flow fields at Q^* = 0.90.

(Fig.3a) and a similar expansion of the high loss region is observed in the same region at this flow rate (Fig.5b). So, despite both shrouded and unshrouded cases revealing similar overall characteristics above Q*=0.9, there are large differences in the internal flow fields of the impeller, and some amount of tip leakage flow improves the flow fields near the casing and delays the onset of a corner separation.

The tip clearance has great influence on pump performance. Figure 3b compares the head-flow characteristic curves of an unshrouded impeller between 0.5mm, 1.0mm and 1.5mm tip clearances. The critical flow rate at stall onset increases substantially with the tip clearance. Since a 0.5mm clearance corresponds to 0.8% of the exit passage height or 0.15% of the blade chord length, the performance of the tested mixed-flow impeller is quite sensitive to tip clearance. However, all head-flow curves below Q*=0.54 are basically independent of the tip clearance, including those in shrouded case S. While the stall is progressive in the largest clearance case U15, the impeller at a small tip clearance stalls abruptly. The pump head at higher flow rates decreases as the tip clearance is enlarged due to an increase in tip leakage loss and corresponding secondary losses, and lower energy transfer associated with smaller effective blade area.

Formation of Jet-Wake Flow

The author (Goto, 1990) had investigated the interaction mechanism of secondary flows and the process of jet-wake flow formation in the present impeller by applying the incompressible version of the Dawes' 3-D Navier-Stokes code (Dawes, 1988). The major conclusions relating with the present study are included in the APPENDIX. Although the numerical computations were carried out at the flow rate of Q*=0.9, they also provide a great deal of useful information to support the discussions on flow phenomena at partial flow rates.

Figure 6 compares experimentally measured exit velocity contours at Q*=0.9. In the shrouded case S, the wake flow settles close to the shroud-suction surface corner (Fig.6a) because of the passage vortex which induces strong secondary flows along the shroud towards the corner. As we can see in Fig.7 (curves with circles), the passage vortex tends to overturn the flow and increases the loading near the shroud. The low momentum fluid accumulated in the corner region is very likely to cause early onset of the corner separation. On the other hand, in the unshrouded case U05, the tip leakage flow displaces the wake flow from the casing-suction surface corner towards the middle passage location (Fig.6b) and under-turns the flow in the tip region (curves with squares in Fig.7). These alterations in flow patterns are considered to be responsible for the increased margin for the onset of the corner separation.

As the tip clearance is increased, the tip leakage flow becomes stronger. However, the wake flow tends to settle closer to the casing-suction surface corner opposing against the tip leakage flow (compare the location of wake region between Fig.6c and Fig.6b), overturning the flow in the casing region (curves with triangles in Fig.7). As is described in the APPENDIX, 3-D Navier-Stokes computations by Goto (1990) have shown that (1) the reverse flow due to the strong tip leakage flow through large clearance promotes the thickening of the casing boundary layer and (2) the wake flow, in this case, settles closer to the casing-suction surface corner because of the strong passage vortex (the secondary flow towards the blade suction side along the casing) developed by the thickened casing boundary layer. Because of this, as the tip clearance is increased, the wake flow settles closer to the corner region and the corner separation is more likely to occur at higher flow rates.

The comparison of exit flow fields between the cases S and U05 at Q*=0.9 (Fig.6a and b) shows that the flow fields are substantially improved by the introduction of a small tip clearance. However, if the flow rate is reduced further, the unshrouded case U05 also reveals the stall onset at Q*=0.54 (Fig.5b). Since the critical flow rate of stall onset (Q*=0.54) is much lower than that of the shrouded case S (Q*=0.87) and the jet-wake flow pattern at Q*=0.9 is so different between these two cases, the mechanism of the stall onset in case U05 looks different from the shrouded case. However, the stall onset was in reality caused by the same mechanism, i.e. by the extensive flow separation at the casing-suction surface corner. The reduction of the flow rate has the same effect on flow fields as the enlargement of the tip clearance, since increased blade loading generates a strong tip leakage flow. The casing boundary layer becomes thick, because of the strong tip leakage reverse flow, and the wake settles closer to the casing-suction surface corner as the flow rate is reduced, because of the strong passage vortex developed by the thickened casing boundary layer. The location of the wake flow observed just before the stall onset (Fig.5a, Q*=0.6) is identical to that in the shrouded case (Fig.4a, Q*=0.9).

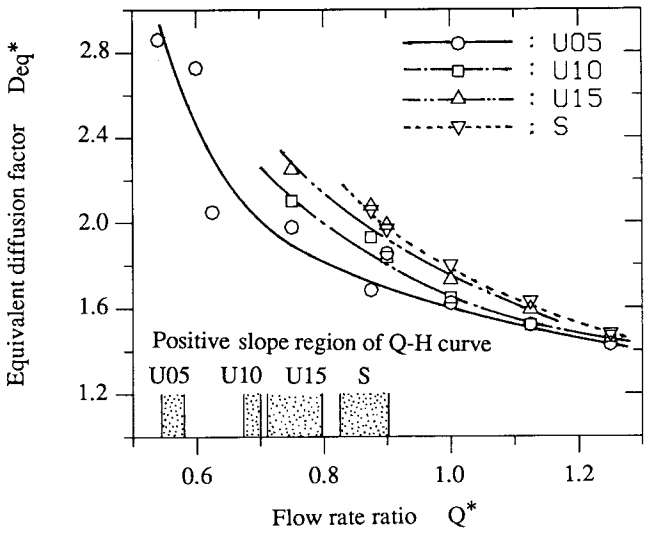

Fig.8 Equivalent diffusion factor.

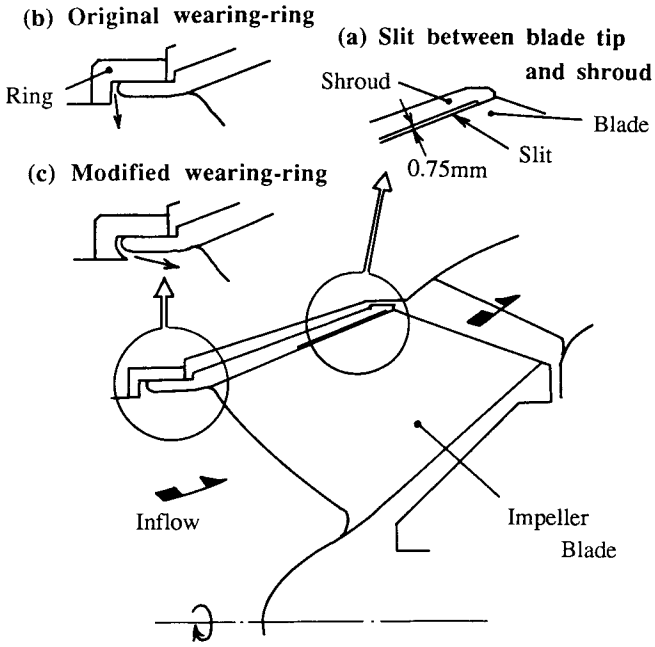

Fig.9 Geometry of modified shrouded impeller.

Equivalent Diffusion Factor

Since it has been clarified that the positively-sloped head-flow curves are caused by the extensive flow separation at the casing-suction surface corner in the impeller, for all cases including the shrouded case, it is interesting to look into the loading limits for the present impeller.

The mixed-flow cascade is mapped into a linear cascade having a stagger angle γ and solidity σ through the following equations.

$$\gamma = \tan^{-1} \{ \sin\phi \cdot (\theta_1 - \theta_2) / (\ln r_2 - \ln r_1) \}$$

$$\sigma = n (\ln r_2 - \ln r_1) / (2\pi \cdot \sin\phi \cdot \cos\gamma)$$

$$\phi = \tan^{-1} \{ (r_2 - r_1) / (z_2 - z_1) \}$$

The values of γ_t and σ_t for the tip section are 70.8 degrees and 1.75 respectively for the present impeller. Then the equivalent diffusion factor D_{eq}* (Lieblein, 1959) is defined as follows.

$$D_{eq}^* = (C_{m1t} \cdot \sin\beta_{2t}) / (C_{m2t} \cdot \sin\beta_{1t}) \cdot (1.12 + 0.01 \cdot i_t^{1.43} + 0.305 \cdot F)$$

$$F = (2 \cdot \sin^2\beta_{1t} / \sigma_t) \cdot \{ 1/\tan\beta_1 - (r_2 \cdot C_{m2}) / (r_1 \cdot C_{m1}) / \tan\beta_2 - (r_1 \cdot \omega) / C_{m1} \cdot (1 - r_2^2 / r_1^2) \}_t$$

where velocity components and flow angles are circumferentially averaged experimental values. Figure 8 shows reasonable correlation between corner stall onset and the equivalent diffusion factor at the tip section, and all cases exhibit positively sloped head-flow curves between D_{eq}*=2.4 and D_{eq}*=2.0. The value of D_{eq}* as the loading limit may vary with a given cascade because the actual deceleration on the blade suction surface depends on the detail of the blade geometry. However, the loading limit obtained here is quite reasonable comparing with the diffusion ratio limit of 2.0 obtained by Lieblein (1959).

Stability Enhancement in Shrouded Case

Shrouded impellers are more widely used than unshrouded impellers for multistage configurations and small machines, since there are difficulties in controlling the latter's tip clearances accurately. As has been pointed out in the previous discussion, the flow pattern within a shrouded impeller tends to cause earlier onset of the corner separation than in unshrouded cases, provided the same blading is adopted for both cases. A passive way to enhance stability under part-load operation was tried for the shrouded case.

In the previous discussions, it has been clarified that the absence of the tip leakage flow is an unfavorable factor of the flow fields

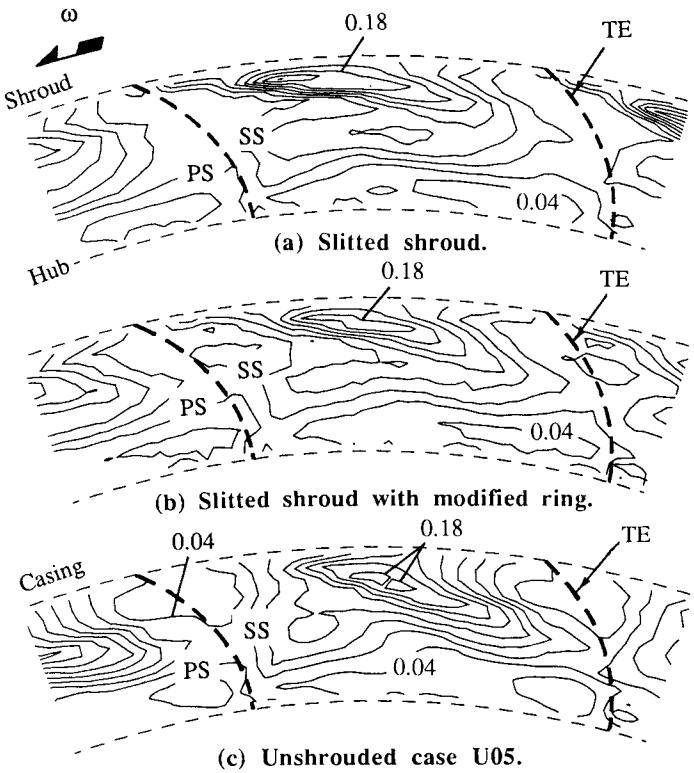

Fig.10 Comparison of exit loss distribution between unshrouded and modified shrouded cases. (Q* = 0.87, Contour interval = 0.02)

within shrouded impeller, since the low kinetic energy fluid tends to migrate in the shroud-suction surface corner and causes earlier onset of the corner separation. Taking this into account, a slit of 0.75mm width (1.2% of the exit blade span) was made between the shroud and the blade tip (Fig.9a) to generate a leakage flow through a slitted shroud. Since the tip leakage flow has also unfavorable effects on flow fields, by causing reverse flows around the leading edge region and thickening the inlet casing boundary layer, the slits were made in the latter half of the impeller between the 50%- and 95%-chord location along the shroud. Another unfavorable factor in flow fields of the shrouded case is the thick inlet boundary layer on the shroud casing due to a leakage flow entering radially inward through a wearing-ring (Fig.9b). Since the extensive corner separation originates in the shroud region, this thickened inlet casing boundary layer is very disadvantageous to corner stall onset. The ring geometry was modified as shown in Fig.9c so that the leakage flow through the wearing-ring would have less velocity components normal to the main inlet flow.

Figure 10 compares the exit flow losses between the shrouded impeller with these two modifications and the unshrouded case U05 at the flow rate of Q*=0.87, whereby case S revealed a stall onset. Substantial reduction in the flow loss is observed by the introduction of the tip leakage flow (Fig.10a). The onset of extensive flow separation has been avoided at this flow rate and the high loss region is quite narrow compared with the case without a slit (Fig.4b). Adoption of the improved wearing-ring in addition to the slit further improves the flow fields. The amount of loss within the wake is reduced even more and the wake flow (high loss region) settles around the midpitch location (Fig.10b) as is in the unshrouded case (Fig.10c). The wake flow in Fig.10b settles closer to the pressure side than the case of Fig.10a because of the thin inlet boundary layer and the resulting relatively weak passage vortex near the shroud (weak secondary flow towards the suction side along the casing).

The comparison of head-flow characteristic curves under these configurations (Fig.11) confirms that a substantial improvement on the stall onset is possible for shrouded impellers by the introduction of a tip leakage flow and a thin inlet casing boundary layer, almost without affecting the characteristics in the higher flow rate region. Thus obtained improvement in the stall margin defined by $(1 - Q^*_{stall})$ is shown in Table 2.

Table 2 Stall margin

Type of impeller	$1 - Q^*_{stall}$
Shrouded case S	0.125
Case S with slit	0.207
Case S with modified ring	0.175
Case S with slit & modified ring	0.302
(Unshrouded case U05	0.46)

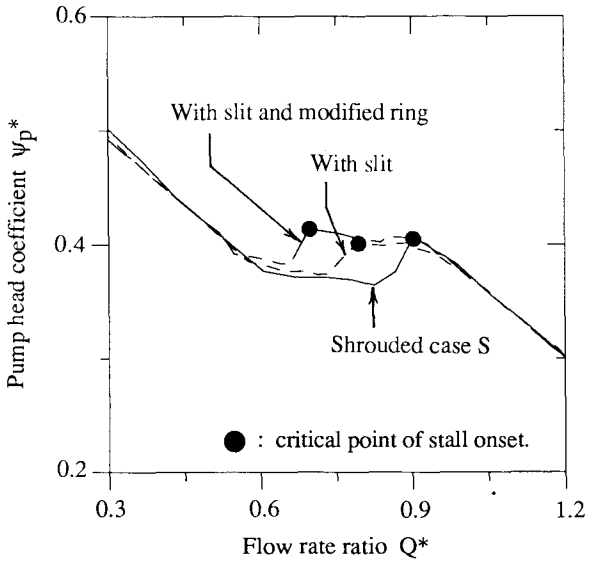

Fig.11 Head-flow characteristics of modified shrouded impeller.

ONSET OF INLET RECIRCULATION

Inlet Recirculation

The inlet flow fields in case U05 were measured using a three-hole cobra probe at three different flow rates (Fig.12). Although a weak reverse flow is observed near the casing at Q*=0.6 (just before the stall onset), the overall inlet flow pattern remains unchanged above this flow rate. However, following a stall at Q*=0.54, a drastic change in the flow field is observed. The meridional velocity distribution shows an extensive recirculating flow region occupying the outer half of the flow passage. The flow in the hub region is accelerated because of blockage due to the flow recirculation near the casing. The recirculating flows convey the angular momentum given by the impeller to the incoming flow, and the flow starts prerotating between a 30%-span and the casing.

Figure 13 shows the development of the inlet recirculation at four different tip clearances. The flow rates where the flow velocity at R_1*=0.97 reveals prerotations of Cu_1*=0.0 (no recirculation), 0.5 (intermediate one) and 0.8 (fully developed one) are plotted in Fig.13 for each tip clearance. The flow regions where positively-sloped head-flow characteristics appeared are also presented in Fig.13. This figure suggests that the onset of extensive corner separation is the triggering mechanism for inlet recirculation in the present impeller. Although the development of recirculation is more progressive for larger tip clearance, fully developed recirculation is observed around Q*=0.54 in every case. It was found by the inlet flow traversing that the flow pattern of fully developed recirculation is independent of tip clearance.

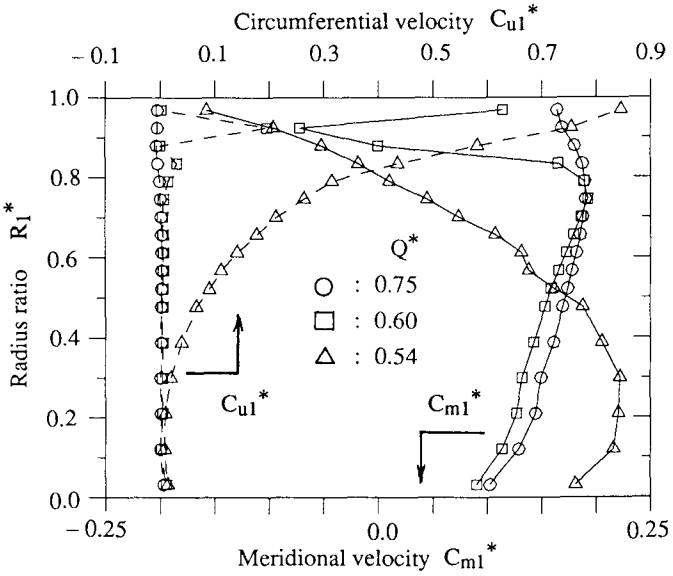

Fig.12 Inlet flow fields in case U05.

Head Generation Mechanism

A comparison of head-flow characteristic curves in Fig.3a shows the difference in the generation mechanism of positively-sloped head-

flow characteristics between shrouded case S and unshrouded case U05. Namely, the increase in flow loss is mainly responsible for the positively-sloped curve at Q*=0.87 in shrouded case S, because Euler's head is nearly equal to that of the unstalled unshrouded case around this flow rate. In contrast, abrupt decrease of Euler's head is observed at Q*=0.54 in unshrouded case U05 (also see ψ_e* curve in Fig.14), suggesting a relatively important role of Euler's head in the production of a positively-sloped curve.

The generation mechanism of positively-sloped head-flow characteristics of the present impeller is investigated based on Euler's equation by a similar method used by Carey et al. (1988). The head generation of Euler's head in an impeller can be attributed to three factors: centrifugal head, dynamic head, and diffusion head as follows.

$$\psi_e^* = (U_2 \cdot C_{u2} - U_1 \cdot C_{u1}) / U_{TE}^2$$
$$= \{(U_2^2 - U_1^2) + (C_2^2 - C_1^2) + (W_1^2 - W_2^2)\} / (2 \cdot U_{TE}^2)$$
Centrifugal Dynamic Diffusion

Figure 14 shows the mass-averaged Euler's head-flow curve and its three components in case U05. Euler's equation holds on each stream surface entering at radius r_1 and leaving at r_2, and the spanwise distribution of Euler's head components around the stall point is plotted in Fig.15 against the exit radius ratio R_2*. Since the onset of inlet recirculation causes drastic change in the radial location of the stream surfaces at the inlet, the peripheral blade speed U_1* on the stream surface, plotted against the exit radius R_2*, varies with the flow rate. After the onset of inlet recirculation at Q*=0.54, there is an abrupt change in the flow field, and the through flow stream lines are shifted remarkably towards the hub at the inlet, due to the large blockage caused by the inlet recirculation. This reduces the peripheral speed U_1 (Fig.15a) and increases the centrifugal effect (Fig.14). However, the overall Euler's head drops at Q*=0.54 because of

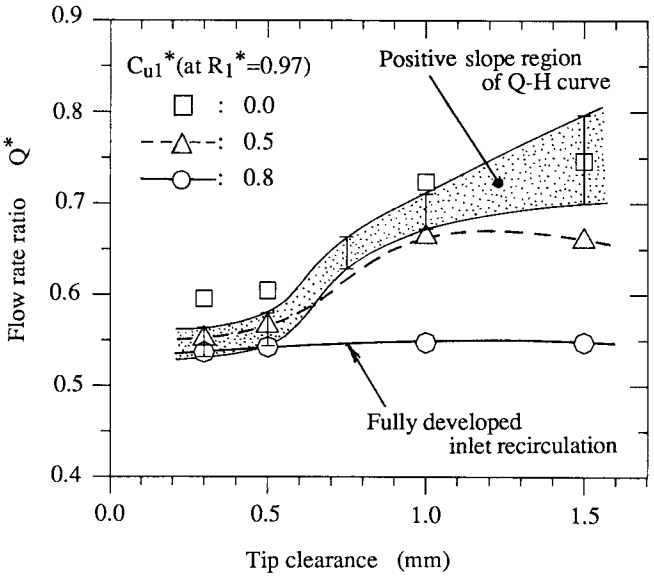

Fig.13 Effect of tip clearance on corner stall onset and inlet recirculation. (Unshrouded impeller)

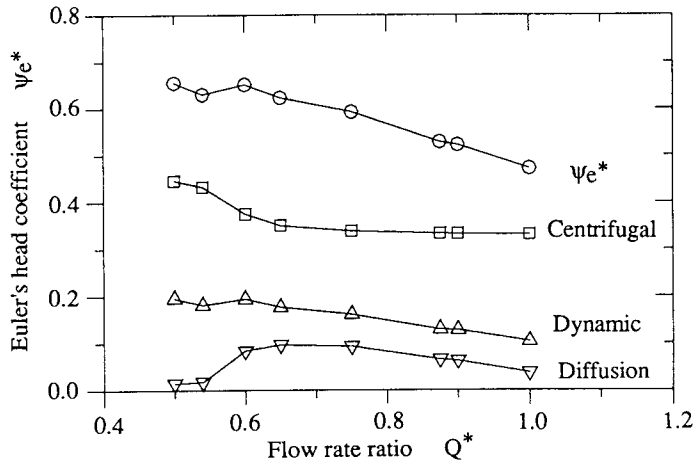

Fig.14 Euler's head in case U05.

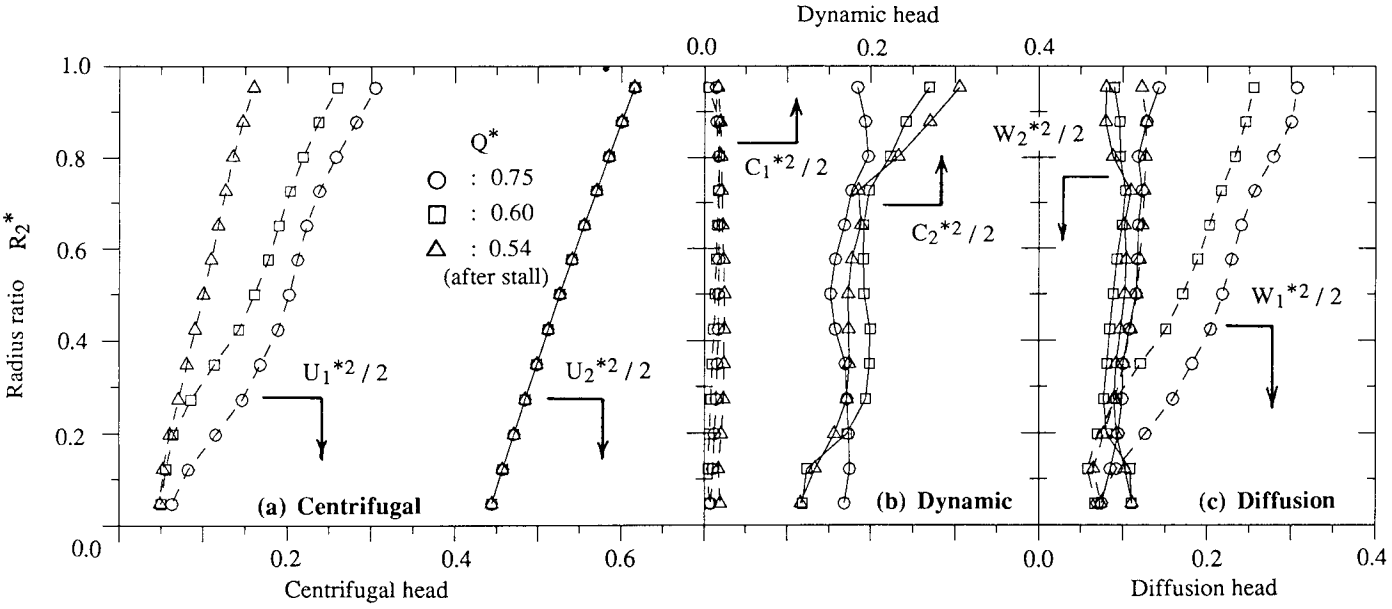

Fig.15 Spanwise distribution of Euler's head components in case U05.

decrease in dynamic and diffusion effects. The large decrease in diffusion head (at Q*=0.54, Fig.14) is not caused by the blade stall but by the reduced inlet relative velocity W_1 (Fig.15c) due to the prerotation and decreased peripheral speed U_1. Once the inlet recirculation is fully developed, the pump shows negatively-sloped head-flow characteristics in all cases because of the increasingly dominating centrifugal effect.

In shrouded case S, the inlet recirculation develops progressively after the stall onset and there is no abrupt change in the flow field at Q*=0.9. Because of this, Euler's head plays a less important role in the shrouded case and the increase in flow losses is the main factor that generate the positively-sloped head-flow characteristic.

CONCLUSIONS

The following conclusions are drawn from the experimental investigation on stall onset and inlet recirculation in a mixed-flow pump impeller for both shrouded and unshrouded cases at various tip clearances.

1) Positively-sloped head-flow characteristic appeared at Q*=0.87 in the shrouded case, and at much lower flow rate of Q*=0.54 in the unshrouded case U05. However, this critical flow rate increased as the tip clearance was enlarged. In all cases, the positively-sloped curves occurred following the onset of extensive flow separation at the shroud-suction surface corner. After the impeller stalled, no evidence of rotating stall was found but instead a region of recirculating flow in the upstream direction at the impeller inlet.

2) In shrouded case S, the low kinetic energy fluid, accumulated in the shroud-suction surface corner due to the strong secondary flows, was responsible for the early onset of the corner separation.

3) In unshrouded cases, the tip leakage flow displaced the wake flow from the corner region towards the midpitch location and increased the stall margin. However, when the tip clearance was large, the strong tip leakage reverse flow thickened the casing boundary layer and developed the passage vortex. In this case, the wake region was located closer to the corner region, because of the strong passage vortex opposing against the tip leakage flow, and the stall margin was decreased.

4) The onset of stall in the shrouded case was substantially delayed by introducing a leakage flow through a slit made between the shroud and the blade tip.

5) The equivalent diffusion factor was found to provide a reasonable basis for determining the loading limit for corner separation onset in the present impeller at different tip clearances.

6) The corner separation was the triggering mechanism for the inlet recirculation. Although the development of recirculation was more progressive for cases with larger tip clearances, the flow pattern of fully developed inlet recirculation was independent of tip clearance.

7) The positively-sloped head-flow curve in the unshrouded case with small tip clearance was caused by two factors: the increase in flow loss, due to the extensive flow separation, and the decrease in Euler's head (reduced diffusion effect), due to the abrupt change of the flow field (extensive inlet recirculation). In the shrouded case, it was mainly caused by the loss increase due to the corner separation, since the development of the inlet recirculation was progressive and there was no abrupt change in the flow pattern which may cause reduction in Euler's head.

ACKNOWLEDGEMENTS

The author would like to express his appreciation to Mr. T. Katsumata for his assistance in setting up the experimental apparatus and conducting the measurements. The author also would like to thank Dr. M. Aoki who offered him useful discussions, and Ebara Research Co., Ltd. for permission to publish this paper.

REFERENCES

Carey, C., Shamsolahi, S., Fraser, S.M. and Wilson, G., 1986, "Comparison of the Three-Dimensional Relative Flow in Two Mixed-Flow Impellers," Proceedings of the IAHR-AIRH Symposium, Vol.2, No.48, Montreal, Canada, September 2-5, 1986.

Carey, C., Fraser, S.M. and McEwen, D., 1988, "Flow Analysis and Part-Load Performance of Model Mixed-Flow Pumps," Proceedings of the International Conference on Part-load Pumping Operation, Control and Behaviour (IMechE 1988-5), Herriot-Watt University, Edinburgh, U.K., September 1-2, 1988.

Dawes, W.N., 1988, "Development of a 3D Navier-Stokes Solver for Application to all Types of Turbomachinery," ASME Paper No. 88-GT-70, Presented at the Gas Turbine and Aeroengine Congress, Amsterdam, The Netherlands, June 6-9, 1988.

Engeda, A., and Rautenberg, M., 1987, "Comparisons of the Relative Effect of Tip Clearance on Centrifugal Impellers," ASME Journal of Turbomachinery, Vol.109, pp.545-549.

Engeda,A., and Rautenberg, M., 1988, "Pump Instabilities at Partial Flow – A Review," Proceedings of the International Conference on Part-load Pumping Operation, Control and Behaviour (IMechE 1988-5), Herriot-Watt University, Edinburgh, U.K., September 1-2, 1988.

Fraser, S.M., Carey, C., and Wilson, G., 1985, "Behavior of Air in the Rotor of a Model Mixed-Flow Pump Operating at Peak Efficiency," ASME Journal of Fluids Engineering, Vol.107, pp.183-190.

Goto, A., 1988, "Phase-locked Measurements of Three-Dimensional Periodic Flow from an Impeller Using a Two-Hole Pitot Probe," Proceedings of the 2nd International Symposium on Fluid Control and Measurements (FLUCOME '88), Sheffield, U.K., September 5-9, 1988.

Goto, A., 1990, "Study of Internal Flows in Mixed-Flow Pump Impellers with Various Tip Clearances using 3D Viscous Flow Computations," ASME Paper No. 90-GT-36, Presented at 1990 ASME TURBO EXPO in Brussels, Belgium, June 11-14, 1990.

Hamkins, C. P., and Flack, R. D., 1987, "Laser Velocimeter Measurements in Shrouded and Unshrouded Radial Flow Pump Impellers," ASME Journal of Turbomachinery, Vol.109, pp.70-76.

Harada, H., 1985, "Performance Characteristics of Shrouded and Unshrouded Impellers of a Centrifugal Compressor," ASME Journal of Engineering for Gas Turbines and Power, Vol.107, pp.528-533.

Howard, J. H. G., and Kittmer, C. W., 1975, "Measured Passage Velocities in a Radial Impeller With Shrouded and Unshrouded Configurations," ASME Journal of Engineering for Power, Vol.97, pp.207-213.

IMechE, 1988, "The International Conference on Part-load Pumping Operation, Control and Behaviour," Held at Herriot-Watt University, Edinburgh, U.K., September 1-2, 1988.

Lenneman, E., and Howard, J. H. G., 1970, "Unsteady Flow Phenomena in Rotating Centrifugal Impeller Passages," ASME Journal of Engineering for Power, Vol.92, pp.65-72.

Lieblein, S., 1959, "Loss and Stall Analysis of Compressor Cascades," ASME Journal of Basic Engineering, Vol.81, pp.387-400.

APPENDIX

The complex three-dimensional flow fields in the present impeller have been investigated numerically by Goto (1990) by applying the incompressible version of the Dawes' 3-D Navier-Stokes code. The computational grid on the meridional plane is shown in Fig.A1, and all computations have been carried out at the flow rate of Q* = 0.9. The applicability of the code has been confirmed by comparison with a variety of experimentally measured jet-wake flow pattern for both shrouded and unshrouded cases at various tip clearances.

The difference in the formation of jet-wake flow pattern between the two cases has been explained by the different way of interaction between secondary flows. Namely, in shrouded case, the wake flow settles at the shroud-suction surface corner because of strong secondary flows along the shroud and the blade suction surface towards the corner region. The introduction of a small tip clearance (unshrouded case) displaces the wake flow from the corner to the middle passage location because of the tip leakage flow and establishes a different jet-wake flow pattern.

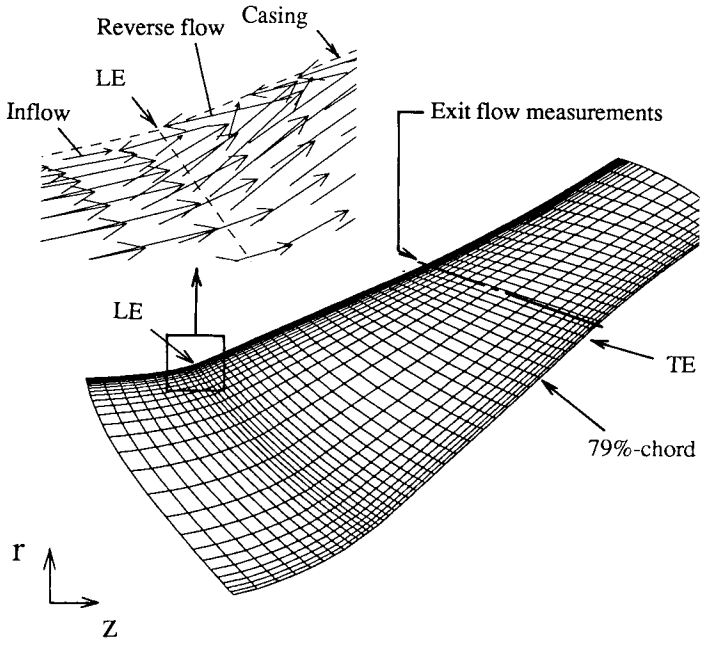

Fig.A1 Meridional computational grid and velocity vectors. (Q*=0.9, Suction side, Unshrouded case U05)

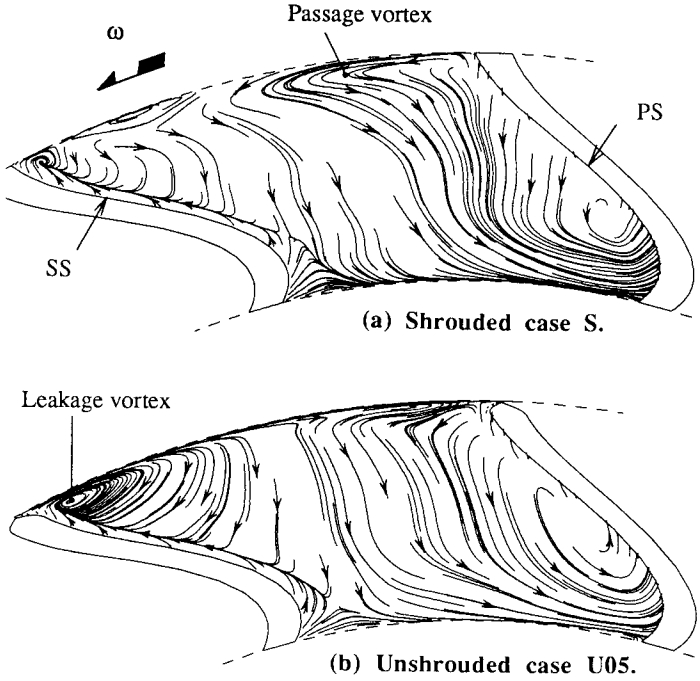

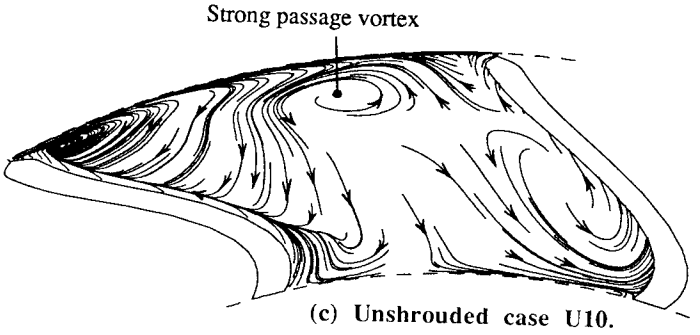

Fig.A3 Particle path lines on quasi-orthogonal plane. (Q*=0.9, at 79%-chord location)

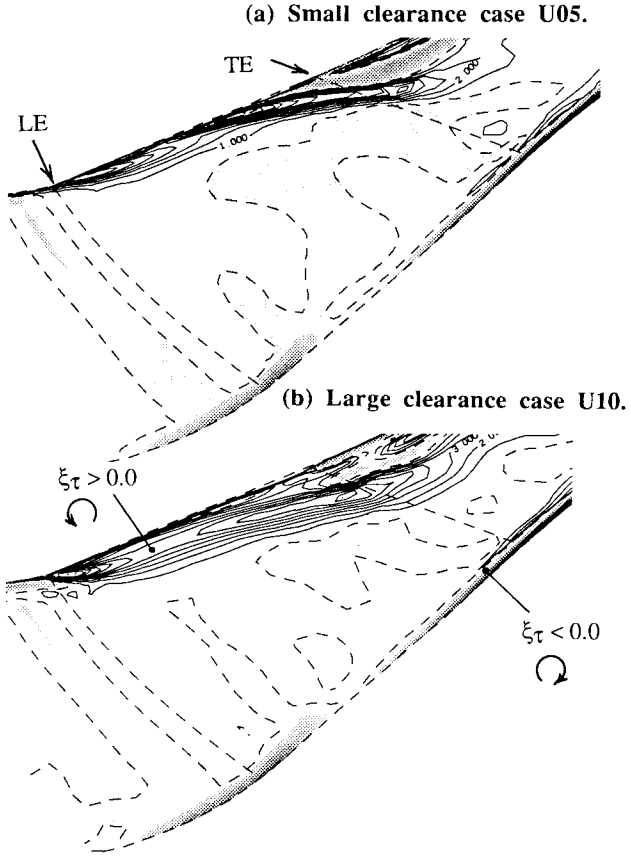

Fig.A2 Casing boundary layer development. (Q*=0.9, Perpendicular vorticity contours, Contour interval = 1.0, Midpitch location)

The tip leakage flow, crossing the blade tip from the pressure side to the suction side of the blade, causes a reverse flow near the casing (Fig.A1). When the tip clearance is enlarged, the strong tip leakage reverse flow interacts with the incoming flow and makes the casing boundary layer thicker. Figure A2 compares the development of the boundary layer on the casing between two different tip clearances in the form of perpendicular vorticity contours. The tip leakage flow becomes strong as the clearance increases. However, the passage vortex (secondary flow along the casing towards the suction side) also develops quickly and becomes strong as is shown in Fig.A3, which compares the different pattern of the secondary flows on a quasi-orthogonal plane at a 79%-chord in the form of particle path lines of secondary flows. The quick development of the passage vortex in the large clearance case is caused by the thick casing boundary layer due to tip leakage induced reverse flows. Consequently, the location of the wake flow, formed in the interaction region between the tip leakage flow and the passage vortex, settles closer to the suction surface as the tip clearance is enlarged.